Atmos. Chem. Phys. Discuss., 14, 21101–21148, 2014
www.atmos-chem-phys-discuss.net/14/21101/2014/
doi:10.5194/acpd-14-21101-2014
© Author(s) 2014. CC Attribution 3.0 License.

Atmospheric Chemistry and Physics Discussions

This discussion paper is/has been under review for the journal Atmospheric Chemistry and Physics (ACP). Please refer to the corresponding final paper in ACP if available.

Scattering and absorption properties of near-surface aerosol over Gangetic–Himalayan region: the role of boundary layer dynamics and long-range transport

U. C. Dumka[1], D. G. Kaskaoutis[2], M. K. Srivastava[3], and P. C. S. Devara[4]

[1]Aryabhatta Research Institute of Observational Sciences, Nainital, India
[2]Department of Physics, School of Natural Sciences, Shiv Nadar University, Tehsil Dadri, India
[3]Department of Geophysics, Banaras Hindu University, Varanasi, India
[4]Amity Institute of Laser Technology & Optoelectronics, Amity University Haryana, Gurgaon, India

Received: 27 June 2014 – Accepted: 31 July 2014 – Published: 18 August 2014

Correspondence to: U. C. Dumka (dumka@aries.res.in; ucdumka@gmail.com)

Published by Copernicus Publications on behalf of the European Geosciences Union.

Abstract

Knowledge of light scattering and absorption properties of atmospheric aerosols is of vital importance in evaluating their types, sources and radiative forcing. This is of particular interest over the Gangetic–Himalayan (GH) region due to large aerosol loading over the plains and the uplift over the Himalayan range causing serious effects on atmospheric heating, glaciology and monsoon circulation. In this respect, Ganges Valley Aerosol Experiment (GVAX) was initiated over the region aiming to examine the aerosol properties, source regions, uplift mechanisms and aerosol-cloud interactions. The present study examines the temporal (monthly, seasonal) evolution of scattering (σ_{sp}) and absorption (σ_{ap}) coefficients, their wavelength dependence, and the role of the Indo-Gangetic plains (IGP), boundary-layer dynamics (BLD) and long-range transport (LRT) in the aerosol uplift over the Himalayas. The measurements are performed at the elevated site Nainital via the Atmospheric Radiation Measurement Mobile Facility including several instruments (Nephelometer, Particle Soot Absorption Photometer, etc.) during June 2011 to March 2012. The σ_{sp} and σ_{ap} exhibit a pronounced seasonal variation with monsoon low and post-monsoon (November) high, while the scattering wavelength exponent exhibits higher values during monsoon, in contrast to the absorption Ångström exponent which maximizes in December–March. The analysis is performed separately for particles bellow 10 and 1 µm in diameter in order to examine the influence of the particle size on optical properties. The elevated-background measuring site provides the advantage of examining the LRT of natural and anthropogenic aerosols from the IGP and southwest Asia and the role of BLD in the aerosol lifting processes, while the aerosols are found to be well-mixed and aged-type dominant.

1 Introduction

Light scattering and absorption by atmospheric aerosol cause reduction in solar radiation reaching the ground and deterioration of visibility and air quality, modifying the

ACPD
14, 21101–21148, 2014

atmosphere's radiative and energy budget (Antón et al., 2012). On the other hand, the backscattering ratio is a crucial parameter for quantifying the cooling effect of aerosols on climate, as it is a measure of the fraction of radiation scattered back to space. Although it is weakly dependent on aerosol concentration, it provides useful information of the refractive index, angular dependence of scattering, size and shape of aerosols (Gopal et al., 2014). Wide-spread aerosol pollution mostly from anthropogenic sources is a common phenomenon over the south Asia, with serious effects on atmospheric circulation, climate and human health (Lawrence and Lelieveld, 2010 and references therein). This aerosol-pollution layer, especially over the Indo-Gangetic Plains (IGP), is clearly observed by the satellite imagery as a thick haze layer (Atmospheric Brown Clouds, ABC) over the region (Di Girolamo et al., 2004; Ramanathan et al., 2007), spreading also over the Himalayas with significant light absorption due to large Black Carbon (BC) concentration (Adhikary et al., 2007; Nakajima et al., 2007; Kopacz et al., 2010; Gautam et al., 2011).

During the last decades, the IGP has experienced increasing aerosol and pollutant emissions mainly from anthropogenic sources, fossil-fuel and bio-fuel combustion and agricultural biomass burning (Lu et al., 2011; Kaskaoutis et al., 2012), which along with the natural dust emissions and long-range transport (LRT) have led to severe turbid atmospheres (Kaskaoutis et al., 2013). As a consequence, aerosols can strongly modify the regional climate via radiative forcing (Ramanathan et al., 2005; Lau et al., 2006; Gautam et al., 2010) and changes in cloud microphysics, monsoon rainfall and dynamics (Randles and Ramaswamy, 2008, Bollasina and Nigam, 2009; Ganguly et al., 2012; Manoj et al., 2011; Dipu et al., 2013). Due to their significant influence on regional weather, climate, monsoon circulation, glaciology and human health, aerosols are systematically examined over Indian Himalayas, mostly focusing on columnar properties and radiative forcing (Dumka et al., 2006, 2008; Hegde et al., 2007; Guleria et al., 2011 and reference therein) and a few studies on aerosol chemistry (Ram et al., 2008, 2010; Hegde and Kawamura, 2012). On the other hand, systematic analysis of near-surface aerosol properties is sparse and mostly performed under an Indian-Finish research

ACPD
14, 21101–21148, 2014

initiative (Hyvärinen et al., 2009, 2011a, b). Furthermore, Raatikainen et al. (2014) examined the influence of boundary-layer dynamics (BLD) and the effect of changes in boundary-layer height (BLH) on aerosol concentrations over the IGP and their transport up to the Himalayas foothills. Panwar et al. (2013) analyzed the PM and BC aerosol mass concentrations at Mukteshwar, while Komppula et al. (2009) and Neitola et al. (2011) focused on the aerosol size distribution and new particle formation at the same site.

To improve the knowledge of radiative properties of atmospheric aerosols, their origin and spatio-temporal distribution over the Gangetic–Himalayan (GH) region, the Ganges Valley Aerosol Experiment (GVAX) was initiated during June 2011 to March 2012. The GVAX project was a joint research campaign between US Department of Energy (DoE) Atmospheric Radiation Measurement (ARM) Program, and Indian Institute of Science, Bangalore conducted at Manora Peak, Nainital, in the central part of Indian Himalayas (29.21° N, 79.27° E, 1958 m a.m.s.l.). More details about the GVAX project and its operation can be found in Kotamarthi and Satheesh (2011), while some initial results have recently been published by Manoharan et al. (2014) and Dumka and Kaskaoutis (2014).

The objective of the present work is to investigate the intensive and extensive properties (scattering and absorption coefficients, their wavelength dependence and relationship between them) of near-surface aerosol over the GH region during the framework of GVAX campaign. Moreover, seasonal and diurnal evolution of absorption and scattering aerosol properties as a function of particle size ($D_{10\,\mu m}$ and $D_{1\,\mu m}$) reveals the specific role of particle size in the optical properties, BLD, uplift of aerosols and LRT. The nearly backgro und measuring site (i.e. Nainital), gives us the possibility of exploring the specific role of aerosol-pollution uplift from the IGP to the Himalayan foothills and the seasonal influence of the LRT on aerosol optical properties.

ACPD
14, 21101–21148, 2014

2 Measurements and data analysis

2.1 Observational site

The aerosol measurements were conducted by DoE/ARM Mobile Facility (AMF) deployed at the mountain-top (1958 m a.m.s.l.) Manora Peak, Nainital, in the GH region (Dumka and Kaskaoutis, 2014). The observational site is far from any major pollution sources, such as industrialized areas and metropolitan cities, with a total population of ∼ 0.5 million (as per census 2011) and population density of ∼ 50 people km^{-2}. The site is bounded by high-altitude mountain peaks in the north and east directions and opens to the IGP region (densely populated, high polluted and aerosol laden) in the south and west. By considering the elevated nature of the site, the growth of planetary boundary layer (PBL) in the late afternoon hours (usually above 3–3.5 km a.m.s.l.) plays a major role in bringing-up aerosols from the IGP, causing significant perturbations in atmospheric physics and chemistry (Dumka et al., 2010; Prabha et al., 2012). The major aerosol sources at Nainital during winter are local/regional biomass-burning emissions (domestic use and heating purposes) and transport of pollutants from the IGP (Dumka et al., 2008). During pre-monsoon (March–June), the site is influenced by transporting dust plumes from Thar desert and southwest Asia (Hegde et al., 2007; Kumar et al., 2014) with a relative decrease in carbonaceous aerosols (Ram et al., 2008), while in post-monsoon, smoke-laden air masses from agricultural crop-residue burning in Punjab affect the site. Rain-washout process during the monsoon period decreases the aerosol concentration.

2.2 Measurements and techniques

In-situ measurements of near-surface aerosol absorption (σ_{ap}) and scattering (σ_{sp}) coefficients were carried out using the aerosol observing system (AOS) (Dumka and Kaskaoutis, 2014 and references therein). The AOS was housed in an air conditioned trailer and aerosol samples were obtained from the top of a stainless steel intake stack

ACPD
14, 21101–21148, 2014

(∼ 21.4 cm inner diameter), protected with a rain cap and a metal screen designed to exclude insects. The aerosols were passed from the stack through a manifold and into several sampling lines that deliver the sample air to the various instruments. Before the light scattering and absorption measurements were made, each aerosol sample passes through an inertial impactor with a cut-off particle diameter at either 1 µm ($D_{1\,\mu m}$) or 10 µm ($D_{10\,\mu m}$). An automated inlet switch operating at 5 min frequency is used to direct the air sample to $D_{1\,\mu m}$ and $D_{10\,\mu m}$ impactors in order to remove the larger particles. The AOS instrumentation that is used in the current work consists of Nephelometer and Particle Soot Absorption Photometer (PSAP) from which several extensive and intensive aerosol properties have been analyzed (see Table 1). Some of them (bold highlighted) are examined in the current work, while others are subjected of further analysis.

The σ_{ap} was measured via the three wavelengths (0.47, 0.53 and 0.66 µm) PSAP. The PSAP uses a filter-based technique in which aerosols are continuously deposited onto a glass fibre filter and the change in the transmitted light is related to the σ_{ap} of the deposited particles using the Lambert Beer's law (Bond et al., 1999). The filter was changed whenever the amount of transmitting light achieved is ∼ 70 % of the initial intensity, while the data averaging time was 1 min. The response of PSAP depends on aerosol loading on the filter, amount of light scattered by particles, flow rate (1.5 L min^{-1}) and spot size (Virkkula et al., 2011). Following the methodology from several previous works (Bond et al., 1999; Virkkula et al., 2011), the raw PSAP data were processed to estimate the σ_{ap} by incorporating the flow and spot size calibrations. The additional biases are due to the scattering and multi-sample loading on the filter, instrument noise (∼ 6 % of total absorption, Bond et al., 2001) and uncertainty in the PSAP measurements (1–4 M m^{-1} for the 1 min averaged data samples, Manoharan et al., 2014). The total uncertainty of the PSAP measurements after the transmission and scattering correction is ∼ 20–30 % (Bond et al., 1999).

The total scattering (σ_{sp}; between 7 and 170°) and hemispheric backscattering (σ_{bsp}; between 90 and 170°) coefficients at three wavelengths (0.45, 0.55 and 0.70 µm) were

ACPD
14, 21101–21148, 2014

measured with an integrating Nephelometer (Model 3563, TSI). The Nephelometer operated at a relative humidity (RH) below 40 % to minimize the effects of changing RH on measurements, while a second Nephelometer was also connected to a humidity scanning system to provide measurements of σ_{sp} and σ_{bsp} as a function of RH for studying the light scattering enhancement factor (work under preparation). The angular non-idealities (i.e. truncation error) and non-Lambertian light source were corrected following the methodology described by Anderson and Ogren (1998) and details given in Dumka and Kaskaoutis (2014 and references therein). These corrections are needed to subtract the light scattering by air molecules, the instrument walls and the detector background noise. The averaging time was set to 1 min, and the Nephelometer was calibrated using CO_2 as high span gas and air as low span gas. On an average, the calibration constant is within ±2 % and the overall uncertainty in the σ_{sp} is ∼ 7 % (Heintzenberg et al., 2006).

The aerosol coefficients σ_{ap}, σ_{bsp} and σ_{sp} measured directly by the AOS are referred to as "extensive properties", because they are mainly pertain to the amount of aerosols in the atmosphere. These measurements were used to determine several other aerosol parameters (known as "intensive properties"), such as hemispheric backscatter fraction (b), up-scatter fraction (β), scattering Ångström exponent (SAE), absorption Ångström exponent (AAE), single scattering albedo (SSA, ω), asymmetry parameter (g), submicron scattering (R_{sp}) and absorption (R_{ap}) fractions, which are involved in the radiative forcing estimations, rather than being related directly to the aerosol loading. Therefore, the intensive properties relate more to the character of aerosols, such as albedo, particle size and hygroscopic behavior. The details of extensive and intensive parameters and the equations used for their calculation are given in Table 1.

ACPD
14, 21101–21148, 2014

3 Results and discussion

3.1 Variations in meteorological parameters

In terms of weather conditions and climatology, the observational site is characterized by four different seasons: winter (December-January-February; DJF), spring/pre-monsoon (March-April-May; MAM), summer/monsoon (June-July-August-September; JJAS) and autumn/post-monsoon (October–November; ON), respectively. During the study period (June 2011 to March 2012), the ambient pressure, temperature (Temp), relative humidity (RH), wind speed (WS) and wind direction (WD) were continuously monitored using the surface meteorological instrumentation (MET) data from the ARM AMF facility.

The ambient atmospheric pressure varies between 79 and 81 Kpa, gradually increasing from monsoon to winter and then, slightly decreasing towards spring (Fig. 1a). The monthly-mean temperature remains nearly steady ($\sim 20\,^{\circ}$C) between June and September, with a gradual decrease thereafter to a minimum value of $\sim 7\,^{\circ}$C in January (Fig. 1b). The RH is greater than 90 % during summer monsoon and decreases to about 60 to 40 % during the remaining period, also exhibiting larger fluctuation due to changing weather conditions involving arrival of humid or dry air masses (Fig. 1c). In general, the wind speed (Fig. 1d) varies between 2 and 6 $\mathrm{m\,s^{-1}}$ with an average of $\sim 2\,\mathrm{m\,s^{-1}}$ for most of the time. Westerly-to-northwesterly winds (Fig. 1e) dominate during October–March period, carrying aerosols and pollutants from western IGP and southwest Asia, as well as dust plumes on certain occasions (Hegde et al., 2007). June is mostly considered as a transition month with changing wind from westerly to easterly, while the mean wind direction from July to September is easterly to south-easterly associated with increased monsoon rainfall.

ACPD
14, 21101–21148, 2014

3.2 Temporal evolution of near-surface aerosol properties

This section analyzes the temporal evolution of near-surface aerosol properties at Nainital and discusses them as a function of wavelength, particle size and prevailing atmospheric and meteorological conditions.

3.2.1 Extensive properties

The mean values (averaged during the entire study period) of spectral σ_{sp}, σ_{bsp} and σ_{ap} for $D_{1\,\mu m}$ and $D_{10\,\mu m}$ are shown in Fig. 2a–c. All the examined parameters show a slight decreasing trend with wavelength, but the largest differences are seen as a function of the particle size, since $D_{10\,\mu m}$ particles exhibit higher scattering, backscattering and absorption as well. On the other hand, the range of all parameters is much larger for $D_{10\,\mu m}$ particles since their size distribution is much more expanded, suggesting larger variation in source regions, mixing processes and optical properties. Although such a behavior is expected for the scattering and backscattering processes via the Mie theory (the larger particles are more efficient scatters especially at longer wavelengths), the higher absorption by the larger particles is an important finding that merits further investigation. In this respect, Manoharan et al. (2014) reported a 30 % greater absorption for $D_{10\,\mu m}$ compared to $D_{1\,\mu m}$ during October–November 2011 (GVAX results), which was found to be the largest difference, since the two particle-size groups exhibit similar absorption efficiency (7.63 ± 5.32 and 6.38 ± 3.91 for $D_{10\,\mu m}$ and $D_{1\,\mu m}$, respectively) during monsoon. The post-monsoon season coincides with the post-harvest agricultural biomass burning period in Punjab, northwestern India (Kaskaoutis et al., 2014), implying that these absorbing aerosols can be also of larger size via mixing processes in the atmosphere (gas-to-particle conversion, coagulation, condensation, ageing) during their transportation up to Nainital. These aerosols are mostly emitted over IGP, whereas the local freshly-emitted aerosols at Nainital (mostly in the $D_{1\,\mu m}$ size group) seem not to affect so much the light absorption due to their significantly lower abundance (Hyvärinen et al., 2009; Ram et al., 2010). It should be noted here

ACPD
14, 21101–21148, 2014

that the difference in absorption efficiency between $D_{10\,\mu m}$ and $D_{1\,\mu m}$ was found to be larger for higher aerosol loading. On the other hand, the scattering is much larger ($\sim 40\,\%$) for the $D_{10\,\mu m}$, especially at longer wavelengths, while the σ_{bsp} exhibits rather neutral wavelength dependence.

The differences in the three parameters, namely, σ_{sp}, σ_{bsp} and σ_{ap} as a function of the particle size are examined via the frequency distribution histograms (Fig. 3a–c). A large difference between the two size groups is seen in the distribution of the σ_{sp} values, whereas the frequency distributions for σ_{bsp} and σ_{ap} are similar for both size groups with larger frequency at higher (lower) values for the $D_{10\,\mu m}$ ($D_{1\,\mu m}$). The average σ_{sp} and σ_{ap} during the whole study period were found to be 177.2 and 10.9 $M\,m^{-1}$, respectively, for the $D_{10\,\mu m}$ and 104.4 and 8.95 $M\,m^{-1}$ for the $D_{1\,\mu m}$, with significant seasonal variation, which is examined in the following. The mean value of σ_{sp} is similar to earlier observations over the site (Pant et al., 2006; Beegum et al., 2009). The σ_{sp} values over central Indian Himalayas (present study and Hyvärinen et al., 2009) are comparable to those found over central India during February 2004 (Jayaraman et al., 2006), but are much lower than those (250–2000 $M\,m^{-1}$) reported at polluted Indian megacities, like Delhi (Ganguly et al., 2006). Lower values of σ_{sp} (97 ± 9.2) $M\,m^{-1}$ and higher of σ_{bsp} ($14 \pm 0.93\,M\,m^{-1}$) at 550 nm compared to Nainital were found at Anantapur in southern India during the period January–December 2011 (Gopal et al., 2014), suggesting dominance of different aerosol types. σ_{sp} value of $75.2 \pm 41.7\,M\,m^{-1}$ at 550 nm was reported by Andreae et al. (2002) at Sde Boker, Israel, which was typical of moderate-polluted continental air masses, while values of 26 and 410 $M\,m^{-1}$ were found for clean and heavy-smog days, respectively, in Los Angeles (Seinfeld and Pandis, 1998). Table 2 summarizes the extensive and intensive aerosol properties over Nainital during the GVAX campaign along with those measured over mountainous sites.

ACPD
14, 21101–21148, 2014

3.2.2 Intensive properties

The monthly values of SAE and AAE determined at three spectral bands are shown in Figs. 4 and 5, respectively, for both $D_{1\,\mu m}$ and $D_{10\,\mu m}$ size groups. Starting from the SAE (Fig. 4), a similar temporal variation is revealed for both size groups, but with much larger values for the $D_{1\,\mu m}$ (mean of 1.21 ± 0.35 at 0.45–0.70 µm) compared to $D_{10\,\mu m}$ (mean of 0.72 ± 0.42 at 0.45–0.70 µm). Their between ratio is nearly constant to 1.68 suggesting that $D_{10\,\mu m}$ particles possess higher scattering at longer wavelengths leading to a more neutral spectrum (Manoharan et al., 2014). Except this, the SAE values are higher at the shorter wavelength bands, suggesting higher decreasing rate of the scattering process at shorter wavelengths, which is expected according to the Mie theory. Thus, despite the fact that $D_{1\,\mu m}$ and $D_{10\,\mu m}$ particles exhibit similar annual pattern either for scattering or for absorption, the values and the wavelength dependence may be quite different. This indicates that although the seasonal variation in aerosol properties may be similar, mostly attributed to changes in weather conditions and associated air masses, the composition of the super-micron and sub-micron aerosols may alter significantly their optical properties and wavelength dependence, even if the initial source remains the same.

The monthly variability depends on the dominant aerosol type, the contribution of local and transported aerosols, the prevailing meteorological conditions and the mixing processes in the atmosphere. The maximum monthly-mean SAE is observed in August (1.11 ± 0.31 and 1.53 ± 0.26 for $D_{10\,\mu m}$ and $D_{1\,\mu m}$, respectively) and, in general, the wavelength dependence of scattering seems to be higher during monsoon. On the other hand, the minimum values are shown in October and November, when the site is under significant influence of the smoke-laden air masses from northwestern India, and both scattering and absorption are at their highest levels (Manoharan et al., 2014; Dumka and Kaskaoutis, 2014). Many studies (Guleria et al., 2011; Dumka et al., 2008; Srivastava et al., 2012) have shown larger columnar values of Ångström exponent (i.e. smaller particles) over IGP and GH regions during the late post-monsoon

ACPD
14, 21101–21148, 2014

and winter seasons due to the dominance of anthropogenic aerosols and biomass burning, and much lower AE values during pre-monsoon and monsoon due to influence of dust. Thus, the current findings seem to deviate from these results, suggesting different characteristics and types of aerosols between surface and vertical. In this respect, Hyvärinen et al. (2009) found lowest values of Aitken-to-Accumulation mode ratio during the pre- and post-monsoon seasons over central Indian Himalayas indicating largest influence of LRT, which was also justified by the highest particle number concentrations (as in the present study). In contrast, during the monsoon season, the Aitken-to-Accumulation ratio was higher due to more efficient removal of accumulation mode by the rain-washout process, implying that the aerosols are less aged and mostly freshly emitted. This explains the larger wavelength dependence of scattering and the highest SAE values during July–September. The lowest SAE in November is an indicator of the abundance of aged aerosols over the site. Furthermore, the local primary emissions are mostly at the Aitken size, thus contributing to the much larger SAE for the $D_{1\,\mu m}$ particles, and to the general increase in SAE during winter due to the influence of bio-fuel burning. Similar values of SAE but with different annual pattern were found in Anantapur, south India with maximum (1.5 ± 0.09) in January and minimum (0.7 ± 0.07) in September (Gopal et al., 2014) indicating significant difference in source apportionment, influence of local emissions and seasonal meteorological conditions between the GH region and the southern peninsula.

The monthly variation of the AAE at the three wavelength bands exhibits similar pattern for both size groups with larger values at shorter wavelengths (Fig. 5). However, the wavelength dependence of the AAE strongly differentiates as a function of season and particle size. It is higher for $D_{10\,\mu m}$ particles and increases from monsoon to winter and pre-monsoon (for both particle groups), suggesting differences in the source regions and dominant aerosol type. The larger values and wavelength dependence of AAE correspond to enhanced contribution of dust and carbonaceous aerosols from biofuel burning, while values of AAE around 1 are characteristic of dominance of fossil fuels (Kirchstetter et al., 2004). The highest wavelength dependence of AAE in March is

ACPD
14, 21101–21148, 2014

a fingerprint of the larger contribution from dust particles either locally emitted or long-range transported. The AAE for the $D_{1\,\mu m}$ is found to be larger (mean of 1.14 ± 0.18 at 0.47–0.60 µm) than that of $D_{10\,\mu m}$ (mean of 1.07 ± 0.20 at 0.47–0.60 µm), with a maximum during December–March (~ 1.3) and minimum during monsoon (~ 1.0). Manoharan et al. (2014) found that the absorption spectrum was much less wavelength dependent for $D_{10\,\mu m}$ particles during October–November, suggesting either a reduction in absorption at 0.47 µm with respect to 0.66 and/or enhanced absorption at 0.66 µm resulting in less difference between 0.47 and 0.66 µm. This indicates that a significant amount of the $D_{10\,\mu m}$ particles contributes to the ambient aerosols that cause an increase in absorption. The AAEs for $D_{1\,\mu m}$ and $D_{10\,\mu m}$ have shown a correlation coefficient of ~ 0.9 and most of the data points lie close to the 1-1 line (Manoharan et al., 2014), suggesting rather consistency in the sources, at least for the absorption capability. The increase in both absorption and scattering coefficients during the last week of October and November due to enhanced biomass burning activity over northwestern India is associated with a weaker wavelength dependence of both scattering (Fig. 4) and absorption (Fig. 5), especially for $D_{10\,\mu m}$ particles, suggesting an abundance of super-micron aerosols that absorb in the whole spectrum (Manoharan et al., 2014).

The frequency distribution of the SAE and AAE for both $D_{1\,\mu m}$ and $D_{10\,\mu m}$ is shown in Fig. 6 along with the mean and median values. The SAE provides information about the average size distribution of the particles. In this respect, the percentage occurrence could be roughly grouped into two categories i.e., SAE <1 (coarse-mode aerosols) and SAE >1 (fine-mode aerosols). The SAE follows an anti-correlation with the coarse-to-fine mode ratio exhibiting much higher values for sub-micron aerosols especially at shorter wavelengths (Andreae et al., 2002). The frequency distribution of SAE clearly differentiates the $D_{1\,\mu m}$ and $D_{10\,\mu m}$ particles, which exhibit means of 1.21 ± 0.35 and 0.71 ± 0.42, respectively. This indicates the large sensitivity of scattering on the particle size that can be used as a measure for the aerosol-type identification. On the other hand, the wide range (~ 0.1–2.4) of SAE values for both particle groups suggests large variability in sources, seasonality and mixing processes at the measuring site, as

ACPD
14, 21101–21148, 2014

shown in Fig. 4. The average value of SAE at 0.45–0.7 µm was found to be 1.02 ± 0.3 at Anantapur (Gopal et al., 2014), which is well within the average values for $D_{1\,\mu m}$ and $D_{10\,\mu m}$ at Nainital.

In contrast to the SAE, the frequency distribution of the AAE shows a more complicated pattern with $D_{1\,\mu m}$ and $D_{10\,\mu m}$ values to strongly overlap. However, $D_{1\,\mu m}$ shows higher values (1.14 ± 0.18), suggesting larger wavelength dependence of the absorption. Similar to Nainital, the frequency distribution of AAE at Kanpur (Giles et al., 2012) showed significant overlap among different aerosol types, suggesting large difficulty in their discrimination based only on absorption properties. A wide range (from 0.16–2.16) in AAE values was also found by Andreae et al. (2002), with a mean of 1.43 ± 0.41, indicative of very contrasting air masses and aerosol absorption efficiencies in arid Israel. Monthly-mean AAE values in the range of 1.0–1.6 are reported for Mukteshwar, near to Nainital (Hyvärinen et al., 2009), exhibiting larger values during winter as also observed in the present study (Fig. 5).

The monthly evolution of the spectral backscatter fraction (b) is shown in Fig. 7 for both particle sizes. The results show that the b is strongly wavelength dependent, with larger values at longer wavelengths (opposite to that found for σ_{sp} and σ_{ap}, SAE and AAE). The larger SAE that was found in monsoon (Fig. 4) indicates particles of smaller size, which is expected to produce more isentropic scattering leading to smaller b values. During post-monsoon and winter, the b increases (except a small decrease in November) reaching its highest value in March suggesting more irregular type of scattering and favoring of backscatter, which is characteristic of the dust particles (Liu et al., 2008). The b is larger at longer wavelengths, especially for the $D_{1\,\mu m}$ particles, since the backscatter wavelength dependence is lower than that of total scattering (Fig. 2) and, therefore, the backscatter-to-total scattering ratio (b) is more enhanced at longer wavelengths.

A slight higher b values are found for the sub-micron particles over Nainital at 0.45 and 0.55 µm, which become significantly higher at 0.7 µm compared to those of $D_{10\,\mu m}$ (Fig. 7). This is because the coarse particles favor the forward scattering (i.e. larger

ACPD
14, 21101–21148, 2014

asymmetry parameter and smaller b) than the smaller particles. On average, the b values at 0.55 µm were found to be 0.067 ± 0.009 for $D_{10\,\mu m}$ and 0.073 ± 0.012 for $D_{1\,\mu m}$, which are much lower than those (0.13 ± 0.09) reported at Anantapur (Gopal et al., 2014), suggesting presence of more aged aerosols and of larger size over Nainital. Backscatter ratio value of 0.13 was reported at the Negev desert, Israel under continental pollution conditions (Formenti et al., 2001; Andreae et al., 2002), while similar values (0.14 ± 0.02) were found for polluted air masses in the northwestern and eastern United States (Anderson et al., 1999; Sheridan and Ogren, 1999). The b at 0.55 µm lies in the range 0.034–0.089 (0.027–0.100) with higher values in March 0.080 ± 0.005 (0.092 ± 0.006) and lower in August 0.054 ± 0.010 (0.058 ± 0.012), where the values inside parentheses represent the $D_{1\,\mu m}$. Previous studies (Carrico et al., 2003; Doherty et al., 2005) have shown that the b values are higher for dust and particles emitted from forest fires than other types of aerosol, while they may be also sensitive to composition (organic content and particle size distribution) of aerosol (Twardowski et al., 2001; Boss et al., 2004).

Figure 8 shows the temporal evolution of the σ_{sp} and σ_{ap} for the sub-micron ($D_{1\,\mu m}$) particles as fraction of the respective efficiencies of $D_{10\,\mu m}$ (i.e. $D_{1\,\mu m}/D_{10\,\mu m}$). Both fractions are below 1, especially for the scattering as was seen in Figs. 2 and 3, suggesting that the particles larger than 1 µm are responsible for the largest fractions of scattering and absorption. The decreasing trend with the wavelength for the sub-micron scattering fraction implies more wavelength sensitivity compared to $D_{10\,\mu m}$, whereas it becomes rather neutral for the absorption, suggesting that the spectral absorption is similar for both $D_{1\,\mu m}$ and $D_{10\,\mu m}$. The sub-micron absorption fraction is higher than that of scattering suggesting that the single scattering albedo would be higher for $D_{1\,\mu m}$. Indeed, in a previous study (Dumka and Kaskaoutis, 2014) we found higher (0.93) SSA for $D_{1\,\mu m}$ compared to that of $D_{10\,\mu m}$ (0.91). The high (> 0.9) SSA values are attributed to the relatively high (7.7 ± 3.4) values of the OC / EC ratio over Nainital suggesting dominance of scattering OC over the absorbing EC (Ram et al., 2010).

ACPD
14, 21101–21148, 2014

Both absorption and scattering sub-micron fractions exhibit a similar pattern with higher values during July–August, which are decreasing in the post-monsoon, increase again in December–January and decrease in March. The larger SAE in monsoon (Fig. 4) implies abundance of fine aerosols (large Aitken-to-Accumulation ratio, Hyvärinen et al., 2009) leading to enhanced sub-micron scattering. The concurrent high values of sub-micron absorption fraction in July–August suggest that either $D_{1\,\mu m}$ particles are more absorbing than the rest of the year or $D_{10\,\mu m}$ would be less absorbing in monsoon. Sub-micron scattering and absorption are sensitive to the local anthropogenic emissions (at the Aitken size) during the monsoon and winter months, thus exhibiting higher fractions compared to the rest of the period. Except of the particle size and shape that mostly define the scattering processes, the aerosol chemical composition plays a vital role in the absorption efficiency. The carbonaceous aerosols were found to contribute about 25 % of the total aerosol mass in Nainital (Ram et al., 2010), while the WSOC / OC (water soluble organic carbon / organic carbon) ratio (0.55 ± 0.15) was found to be larger than that over the IGP locations, suggesting enhanced contribution from secondary organic aerosols (mostly in the Aitken size). Concerning the coarse-mode particles, except of the LRT dust from the arid and semi-arid regions in southwestern Asia, dust particles may originate from local wind-blown dust, dust re-suspension due to road traffic or dust from farming activity over the GH region (Raatikainen et al., 2014).

3.3 Diurnal cycle of aerosol properties

The monthly-mean diurnal evolutions of σ_{sp}, σ_{ap}, SAE and AAE are shown in Fig. 9a–d, respectively, for both $D_{1\,\mu m}$ and $D_{10\,\mu m}$. The σ_{sp} and σ_{ap} exhibit similar diurnal and seasonal patterns, with post-monsoon to winter (and March) highs and monsoon lows. Both maxima are observed in November due to significant influence of transported smoke from agricultural burning (Dumka and Kaskaoutis, 2014), while a slight decrease is observed in January. The particle size seems to play an important role in both processes, resulting in higher scattering and absorption for particles larger than

ACPD
14, 21101–21148, 2014

1 µm during periods of high aerosol loading. Aerosol scattering and absorption over Nainital is dominated by the concurrent contribution of soil or desert dust in the coarse fraction, and the anthropogenic sulfate and carbonaceous aerosols in the fine fraction. The factor that seems to contribute to the increase in σ_{sp} and σ_{ap} during noon to afternoon hours, is the slope up-stream of the polluted air masses coming from the IGP after deepening (> 2.5–3 km) of the PBL over the Ganges valley. Local-scale daily wind patterns, like valley wind cells, may also influence the diurnal patterns of spectral σ_{sp} and σ_{ap}; upslope winds are expected to increase the aerosol loading over the site, while downslope winds result in atmospheric cleansing. Furthermore, synoptic-scale transport and changing air-mass origin affect the aerosol loading over the Himalayan sites (Xu et al., 2014; Bucci et al., 2014). The annual variation of the σ_{ap} seems to follow that of the BC mass fraction, which was found to be ∼ 1 % during monsoon and 7.6 % during winter (Ram et al., 2010), associated with variation in σ_{ap} (at 0.678 µm) from 0.9 to 33.9 M m^{-1}. However, no significant difference in σ_{ap} and σ_{sp} was found between weekdays and weekends in contrast to Indian cities where a 7.8 % reduction in σ_{sp} was reported in weekends (Gopal et al., 2014).

Similar annual variation of σ_{sp} was found at Mukteshwar, close to Nainital, with July–August lows (25–36 M m^{-1}) and February (94 Mm^{-1}) and April–June highs (Hyvärinen et al., 2009). They also reported lower winter (December–January) values mostly because the IGP pollution layer was trapped below the site altitude, as well as several peaks in post-monsoon due to influence of smoke plumes from agricultural crop-residue burning in northwestern India. A marked annual cycle with higher values during March–June and October–November was observed for the σ_{ap} over Mukteshwar (Hyvärinen et al., 2009), while the lowest values were observed during monsoon and December–January, similar to the present study. Afternoon-to-evening peaks in σ_{sp} and σ_{ap} were also reported at Mukteshwar during the post-monsoon and winter seasons, which are vanished during monsoon (Hyvärinen et al., 2009). However, these diurnal patterns differentiate than those found over Indian cities, where two prominent peaks (morning and evening) are observed (Ganguly et al., 2006; Gopal et al., 2014).

ACPD
14, 21101–21148, 2014

The seasonal pattern of SAE reveals larger values during monsoon, which can be explained by the rain washout of the coarser aerosols, and a secondary increase during December–January mostly associated with local emissions from biofuel combustion (morning and evening maxima). The diurnal variation observed in December–January is smoothed during the rest of the year for both particle groups. In contrast to SAE, the diurnal pattern of AAE exhibits significant variability during October–March, indicating dominance of different aerosol types and mixing processes. Higher AAE values (> 1.3–1.4) are observed during night-to-early morning hours in the winter season, while during noontime the AAE goes down to 1–1.2. Peaks in AAE during the morning and evening hours were also found over Mukteshwar (Hyvärinen et al., 2009) suggesting influence of local biomass burning i.e. burning of leaves and wood for heating, which were not so obvious in the diurnal patterns of σ_{sp} and σ_{ap} (Fig. 9a and b) because they are mostly affected by the LRT from IGP. The diurnal pattern of AAE reveals the influence of different aerosol sources and combustion processes, i.e. local emissions from biofuel burning in the early morning and evening (high values of AAE) and transport of mostly aged aerosols from fossil-fuel combustion in IGP during noon to early afternoon (low values of AAE) (Bergstrom et al., 2007). In contrast, any diurnal pattern flattens out during monsoon, when the low AAE values (below 1) are associated with lowest σ_{ap}.

Raatikainen et al. (2014) noted that the air masses up to Himalayan sites in winter travel at higher altitudes than the maximum BLH (~ 1–1.5 km) over the IGP, thus not being able to carry significant amount of aerosol and pollutants. Such pollution transportation is very much favored during pre-monsoon when the BLH is at its maximum (> 3–3.5 km) and the dilution of aerosols in the vertical favors their uplift to Himalayan foothills. As a consequence, the role of the IGP to the aerosol concentrations over the Himalayas is strongly related to BLH and dynamics (Raatikainen et al., 2014). However, the rain washout during monsoon strongly reduces the aerosol concentrations and seems to be the most effective scavenging factor that controls the aerosol loading and evolution.

ACPD
14, 21101–21148, 2014

3.4 The role of wind and LRT in aerosol properties

The seasonal variation in the aerosol composition and optical properties over Nainital is a function of the emission sources, meteorological conditions (rainfall, wind pattern) and LRT. In this respect, the σ_{sp}, σ_{ap}, SAE and AAE are examined against the wind speed and direction (Fig. 10). In general, the results show that the west/southwest flow enhances the scattering and absorption coefficients, while the northern (coming from Tibetan Plateau) and east air masses are usually clean. The air masses from southeast direction are mostly associated with the monsoonal flow, higher rainfall and lower aerosol concentrations; however, it was found that the concentrations from this sector are similar to southwest during the other seasons. Similar findings (lower values for both scattering and absorption associated with east/southeast directions) were found at Mukteshwar (Hyvarinen et al., 2009), while the highest values were found for western and southwestern sectors. The maximum σ_{sp} and σ_{ap} values are mostly associated with moderate winds (4–6 ms^{-1}), supporting the higher contribution of the transported aerosols at the observational site. In contrast, the accumulation of pollutants over the urban areas is favored by calm winds resulting in larger values of the σ_{sp} (almost double for wind speed $< 0.5\,m\,s^{-1}$ compared to wind speed $> 3\,m\,s^{-1}$) at Anantapur (Gopal et al., 2014).

The valley-breeze circulation was found to have a strong impact on the aerosol composition even at the high-altitude (5079 m) Nepal Climate Observatory – Pyramid site in the Everest area (Decesari et al., 2010) and, therefore, can be considered as the major mechanism for the aerosol transport from the polluted IGP up to Himalayas. This was further supported by chemical analysis of the WIOC / EC ratios between Nainital and IGP (Ram and Sarin, 2010), which showed great similarities and aerosol of similar sources. The east flow carries smaller particles with SAE greater than 1.2, which can be up to 1.6–1.8 for certain air masses from southeast; in contrast, the northwest sector is associated with larger particles (much lower values of SAE). However, the AAE is not so much dependent on the wind direction, revealing larger impact of the local

ACPD
14, 21101–21148, 2014

emissions as discussed in Fig. 9. Combination of the results (Figs. 4, 5, 9, and 10) establishes that the influence of the source region and LRT play the major role in the aerosol field and evolution over Nainital in all seasons except monsoon, when the rain washout is the main process.

The BLH over the site was found to exhibit a significant diurnal variation (not presented) ranging from lower than 100 m during cold nights to up to 2 km during noontime in March. The BLH estimated via radio-sonde measurements at Nainital during GVAX (4 profiles per day, around 05:30, 11:30, 17:30 and 23:30 LST) was found to range from ~ 1150 m, on average, during monsoon and post-monsoon to ~ 1550 m during March. Therefore, the BLD play a crucial role in aerosol properties on daily (majorly) and seasonal basis. For longer time intervals (e.g. month, season), the changing air masses carrying aerosols of different origin and characteristics is the main factor influencing the aerosol field.

3.5 Relationship among aerosol parameters

Correlation between different aerosol properties is able to reveal specific characteristics and modification processes in the aerosol field at the observational site. The scatter plot of σ_{sp} vs. σ_{ap} for the two size groups (Fig. 11) shows a strong correlation suggesting covariance in the scattering and absorption properties, which is stronger for the $D_{10\,\mu m}$ (larger slope value), since the scattering effect enhances for the coarse particles. The scatter plot also reveals higher absorption capability for the large particles, which is well documented in the work by Manoharan et al. (2014). For a certain absorption value, the scattering of $D_{10\,\mu m}$ particles seems to be larger than that of $D_{1\,\mu m}$ for σ_{sp} values above 200 $M\,m^{-1}$ indicating that for clean atmospheres the discrimination of the optical properties between coarse and sub-micron aerosols is really difficult.

Correlation of properties related to aerosol loading with those related to particle size is a common way to discriminate between different aerosol types (Kaskaoutis et al., 2010). In this respect, Fig. 12 correlates the σ_{sp} and σ_{ap} with the SAE and AAE,

ACPD
14, 21101–21148, 2014

respectively, for both particle sizes revealing a general decrease in SAE with increasing σ_{sp}. This suggests an increase in size and ageing processes in aerosols (condensation, coagulation) under more turbid atmospheres (Sinha et al., 2012). The respective scatter plots for absorption result in similar findings, but the large scatter in data points does not allow the extraction of safe conclusions about the dominant aerosol, suggesting a rather mixing during the whole campaign period. Changing in chemical composition and humidity impacts may also influence the intensive and extensive properties of aerosols. Such variations usually occur in south Asia and along with alteration in meteorology strongly influence the aerosol concentration and properties (Léon and Legrand, 2003).

Many studies (Eck et al., 2010; Russell et al., 2010; Giles et al., 2012; Vijayakumar et al., 2012; Vijayakumar and Devara, 2014) have suggested the use of correlations between the aerosol absorption and scattering properties for the determination of different aerosol types. In such an approach, we correlate the SAE with AAE for the whole set of measurements at Nainital for both $D_{1\,\mu m}$ and $D_{10\,\mu m}$ groups (Fig. 13). Such a graph is able to reveal the existence of different aerosol types, since the wavelength dependence of scattering and absorption differentiates for the various types. As far as the scattering is concerned, the fine-mode aerosols (biomass burning, soot, urban/industrial emissions) exhibit higher values, while sea-salt and desert dust show lower values of SAE. The AAE is commonly used for aerosol characterization with values around 1 to correspond to vehicle exhausts or fossil fuel combustions, whereas the AAE values in excess of biomass burning or dust aerosol are around 2 or even more (Kirchstetter et al., 2004; Bergstrom et al., 2007). Using AERONET retrievals, Russell et al. (2010) found AAE values varying between 1.2 and 3.0 for dust, 0.75 and 1.3 for urban/industrial, and 1.2 and 2.0 for biomass burning. The range of these values seems to be significant and at the same magnitude (1.2–1.8) to those reported by Eck et al. (2010) for mixtures of dust, smoke and pollution. The current results reveal a rather well mixed atmosphere without clear identification of specific aerosol types, as was found over Kanpur during pre-monsoon (TIGERZ campaign, Giles et al., 2011).

ACPD
14, 21101–21148, 2014

The SAE and AAE are somewhat homogeneously distributed around the mean values of SAE (0.9–1.1) and AAE (1–1.2), while few cases present large values of SAE associated with AAE of 1.0–1.5 revealing the presence of carbonaceous aerosols of mixed fossil and biofuel combustions.

4 Conclusions

A comprehensive analysis of several extensive and intensive properties (total scattering, backscattering, light absorption and their wavelength dependence) of near-surface aerosols was performed in the current study, aiming to investigate the temporal evolutions, variety of aerosol types and influence of transported plumes. The measurements via AMF were made in the framework of GVAX campaign during June 2011–March 2012 at Nainital, located in the foothills of central Indian Himalayas. More specifically, the light scattering and absorption measurements, using three wavelengths integrated Nephelometer and PSAP, were analyzed along with meteorological parameters at the experimental site. The main findings of the study are summarized as follows:

1. the meteorological field exhibited a seasonal-changing pattern, which along with the boundary layer dynamics and the upslope valley winds control the temporal evolution and the aerosol characteristics at Nainital. The surface wind showed a clear dominance of the northwest (winter and pre-monsoon) and southeast (summer monsoon) directions.

2. The scattering coefficient showed higher values during November and March due to the significant influence of biomass-burning aerosols and dust mixed with anthropogenic pollution, respectively, both uplifting from Ganges valley and northwestern India. The absorption coefficient followed a similar pattern, while both parameters exhibited very low values during monsoon due to rain washout process.

ACPD
14, 21101–21148, 2014

3. The wavelength dependence of scattering and absorption, which is defined via the Ångström exponents of scattering (SAE) and absorption (AAE), respectively, exhibited a marked seasonal variation, with monsoon high for SAE and late winter-to-March high for AAE. The higher values of SAE during monsoon may be related to rain washout and the removal of the coarser aerosol particles, while a secondary increase of SAE during winter was associated with local emissions from bio-fuel combustion. The latter seems to have an effect in increasing AAE values during the same period, in association with increased dust occurrence in March.

4. The particle size played a major role in the scattering coefficient and SAE, while its effect was much lesser in absorption processes. Thus, the absorption fraction by the sub-micron particles ($< 1\,\mu m$) was about 0.9 of that of $< 10\,\mu m$ particles, while the respective scattering fraction was only 0.6.

5. The diurnal variation of both scattering and absorption coefficients revealed a noon-to-early afternoon maximum, which was clearly defined during October to March, while it was negligible during monsoon. This suggests that the higher aerosol concentrations were mostly attributed to transport of air masses from the Ganges valley and not to local emissions, while the rain washout effect modulates the diurnal cycle. Furthermore, the diurnal patterns of SAE and AAE revealed that the local emissions, mostly observed during early morning and evening hours, increased both parameters during these parts of the day. This suggests that the local emissions, although they did not have a clear signal in scattering and absorption coefficients, showed different characteristics than the transported air masses from the Ganges valley and affect mostly the aerosol intensive properties.

6. The highest values for both scattering and absorption were associated with south-west air flow, suggesting strong influence of transported aerosols from northwestern India, which were found to have lower SAE values.

ACPD
14, 21101–21148, 2014

7. Analysis of the correlations between the aerosol properties showed that a well-mixed aerosol field dominated over the site, whereas a specific aerosol type can be detected only in a few cases. This suggests the influence of well-mixed and aged polluted air masses over the GH region.

In summary, analysis of the aerosol optical properties revealed that Nainital, although its elevated terrain and remoteness from urban and industrialized regions, usually receives substantial amounts of anthropogenic aerosols, in addition to mineral dust and biomass burning, rendering the site moderately polluted (see Table 2). Most of the aerosol is long-range transported from the Ganges valley and southwest Asian regions. This supports the diurnal pattern of the scattering and absorption coefficients that revealed higher values during noon-to-early afternoon hours associated with higher mixing depth and up-slope of pollutants. Local emissions were found to partly contribute to the aerosol loading and evolution, mostly defined via bio-fuel combustion during the winter season (morning and evening peaks in the AAE).

Acknowledgements. We thank the US Department of Energy for deploying the Atmospheric Radiation Measurements Climate Research Facility. We are grateful to the technical staff of Atmospheric Radiation Measurements for providing valuable data. This study is carried out under GVAX project in collaboration among the DoE, IISc, SPL, ISRO and ARIES. We would like to thank the participants (scientists and technical staff) of the campaign for valuable support. Thanks are also due to the Editor and anonymous reviewers for their insightful comments and valuable suggestions, which improved the scientific content and clarity of the paper.

References

Adhikary, B., Carmichael, G. R., Tang, Y., Leung, L. R., Qian, Y., Schauer, J. J., Stone, E. A., Ramanathan, V., and Ramana, M. V.: Characterization of the seasonal cycle of south Asian aerosols: a regional-scale modeling analysis, J. Geophys. Res., 112, D22S22, doi:10.1029/2006JD008143, 2007.

Anderson, T. L. and Ogren, J. A.: Determining aerosol radiative properties using the TSI 3563 integrating Nephelometer, Aerosol Sci. Tech., 29, 57–69, 1998.

ACPD
14, 21101–21148, 2014

Anderson, T. L., Covert, D. S., Wheeler, J. D., Harris, J. M., Perry, K. D., Trost, B. E., Jaffe, D. J., and Ogren, J. A.: Aerosol backscatter fraction and single scattering albedo: measured values and uncertainties at a coastal station in the pacific north west, J. Geophys. Res., 104, 793–807, 1999.

Andreae, T. W., Andreae, M. O., Ichoku, C., Maenhaut, W., Cafmeyer, J., Karnieli, A., and Orlovsky, L: Light scattering by dust and anthropogenic aerosol at a remote site in the Negev Desert, Israel, J. Geophys. Res., 107, 4008, doi:10.1029/2001JD900252, 2002.

Antón, M., Valenzuela, A., Cazorla, A., Gil, J. E., Fernández-Gálvez, J., Lyamani, H., Foyo-Moreno, I., Olmo, F. J., and Alados-Arboledas, L.: Global and diffuse shortwave irradiance during a strong desert dust episode at Granada (Spain), Atmos. Res., 118, 232–239, doi:10.1016/j.atmosres.2012.07.007, 2012.

Beegum, S. N., Moorthy, K. Krishna, Babu, S. S., Satheesh, S. K., Vinoj, V., Badarinath, K. V. S., Safai, P. D., Devara, P. C. S., Singh, S., Vinod, Dumka, U. C., and Pant, P.: Spatial distribution of aerosol black carbon over India during pre-monsoon season, Atmos. Environ., 43, 1071–1078, doi:10.1016/j.atmosenv.2008.11.042, 2009.

Bergstrom, R. W., Pilewskie, P., Russell, P. B., Redemann, J., Bond, T. C., Quinn, P. K., and Sierau, B.: Spectral absorption properties of atmospheric aerosols, Atmos. Chem. Phys., 7, 5937–5943, doi:10.5194/acp-7-5937-2007, 2007.

Bollasina, M. and Nigam, S.: Absorbing aerosols and pre-summer monsoon hydroclimate variability over the Indian subcontinent: the challenge in investigating links, Atmos. Res., 94, 338–344, doi:10.1016/j.atmosres.2009.06.008, 2009.

Bond, T. C.: Spectral dependence of visible light absorption by carbonaceous particles emitted from coal combustion, Geophys. Res. Lett., 28, 4075–4078, 2001.

Bond, T. C., Anderson, T. L., and Campbell, D.: Calibration and intercomparison of filter-based measurements of visible light absorption by aerosols, Aerosol Sci. Tech., 30, 582–600, 1999.

Boss, E., Pegau, W. S., Lee, M., Twardowski, M., Shybanov, E., Korotaev, G., and Baratange, F.: Particulate backscattering ratio at LEO 15 and its use to study particle composition and distribution, J. Geophys. Res., 109, C01014, doi:10.1029/2002JC001514, 2004.

Bucci, S., Cagnazzo, C., Cairo, F., Di Liberto, L., and Fierli, F.: Aerosol variability and atmospheric transport in the Himalayan region from CALIOP 2007–2010 observations, Atmos. Chem. Phys., 14, 4369–4381, doi:10.5194/acp-14-4369-2014, 2014.

ACPD
14, 21101–21148, 2014

Carrico, C. M., Kus P., Rood M. J., Quinn P. K., and Bates T. S.: Mixtures of pollution, dust, sea salt, and volcanic aerosol during ACE-Asia: radiative properties as a function of relative humidity, J. Geophys. Res., 108, 8650, doi:10.1029/2003JD003405, 2003.

Decesari, S., Facchini, M. C., Carbone, C., Giulianelli, L., Rinaldi, M., Finessi, E., Fuzzi, S., Marinoni, A., Cristofanelli, P., Duchi, R., Bonasoni, P., Vuillermoz, E., Cozic, J., Jaffrezo, J. L., and Laj, P.: Chemical composition of PM_{10} and PM_1 at the high-altitude Himalayan station Nepal Climate Observatory-Pyramid (NCO-P) (5079 m a.s.l.), Atmos. Chem. Phys., 10, 4583–4596, doi:10.5194/acp-10-4583-2010, 2010.

Di Girolamo, L., Bond, T. C., Bramer, D., Diner, D. J., Fettinger, F., Kahn, R. A., Martonchik, J. V., Ramana, M. V., Ramanathan, V., and Rasch, P. J.: Analysis of Multi-angle Imaging Spectroradiometer (MISR) aerosol optical depths over greater India during winter 2001–2004, Geophys. Res. Lett., 31, L23115, doi:10.1029/2004GL021273, 2004.

Dipu, S., Prabha Thara, V., Pandithurai, G., Dudhia, J., Pfister, G., Rajesh, K., and Goswami, B. N.: Impact of elevated aerosol layer on the cloud macrophysical properties prior to monsoon onset, Atmos. Environ., 70, 454–467, 2013.

Doherty, S. J., Quinn, P. K., Jefferson, A., Carrico, C. M., Anderson, T. L., and Hegg, D.: A comparison and summary of aerosol optical properties as observed in situ from aircraft, ship, and land during ACE-Asia, J. Geophys. Res., 110, D04201, doi:10.1029/2004JD004964, 2005.

Dumka, U. C. and Kaskaoutis, D. G.: In-situ measurements of aerosol properties and estimates of radiative forcing efficiency over Gangetic–Himalayan region during the GVAX field campaign, Atmos. Environ., 94, 96–105, doi:10.1016/j.atmosenv.2014.05.021, 2014.

Dumka, U. C., Satheesh, S. K., Pant, P., Hegde, P. and Krishna Moorthy, K.: Surface changes in solar irradiance due to aerosols over central Himalayas, Geophys. Res. Lett., 33, L20809, doi:10.1029/2006GL027814, 2006.

Dumka, U. C., Krishna Moorthy, K., Satheesh, S. K., Sagar, R., and Pant, P.: Short-period modulations in aerosol optical depths over the central Himalayas: role of mesoscale processes, J. Appl. Meteorol. Clim., 47, 1467–1475, doi:10.1175/2007JAMC1638.1, 2008.

Dumka, U. C., Krishna Moorthy, K., Kumar, R., Hegde, P., Sagar, R., Pant, P., Singh, N., and Babu, S. S.: Characteristics of aerosol black carbon mass concentration over a high altitude location in the central Himalayas from multi-year measurements, Atmos. Res., 96, 510–521, ISSN 0169–8095, doi:10.1016/j.atmosres.2009.12.010, 2010.

Eck, T. F., Holben, B. N., Sinyuk, A., Pinker, R. T., Goloub, P., Chen, H., Chatenet, B., Li, Z., Singh, R. P., Tripathi, S. N., Reid, J. S., Giles, D. M., Dubovik, O., O'Neill, N. T., Smirnov, A.,

ACPD
14, 21101–21148, 2014

Wang, P., and Xia, X.: Climatological aspects of the optical properties of fine/coarse mode aerosol mixtures, J. Geophys. Res., 115, D19205, doi:10.1029/2010JD014002, 2010.
Formenti, P., Andreae, M. O., Andreae, T. W., Ichoku, C., Schebeske, G., Kettle, J., Maenhaut, W. Cafmeyer, J., Ptasinsky, J., Karnieli, A., and Lelieveld, J.: Physical and chemical characteristics of aerosols over the Negev Desert (Israel) during summer 1996, J. Geophys. Res., 106, 4871–4890, 2001.
Ganguly, D., Jayaraman, A., Rajesh, T. A., and Gadhavi H: Wintertime aerosol properties during foggy and non foggy days over urban center Delhi and their implications for shortwave radiative forcing, J. Geophys. Res., 111, D15217, doi:10.1029/2005JD007029, 2006.
Ganguly, D., Rasch, P. J., Wang, H., and Yoon, J. H.: Climate response of the South Asian monsoon system to anthropogenic aerosols, J. Geophys. Res., 117, D13209, doi:10.1029/2012JD017508, 2012.
Gautam, R., Hsu, N. C., and Lau, K.-M.: Premonsoon aerosol characterization and radiative effects over the Indo–Gangetic plains: implications for regional climate warming, J. Geophys. Res., 115, D17208, doi:10.1029/2010JD013819, 2010.
Gautam, R., Hsu, N. C., Tsay, S. C., Lau, K. M., Holben, B., Bell, S., Smirnov, A., Li, C., Hansell, R., Ji, Q., Payra, S., Aryal, D., Kayastha, R., and Kim, K. M.: Accumulation of aerosols over the Indo-Gangetic plains and southern slopes of the Himalayas: distribution, properties and radiative effects during the 2009 pre-monsoon season, Atmos. Chem. Phys., 11, 12841–12863, doi:10.5194/acp-11-12841-2011, 2011.
Giles, D. M., Holben, B. N., Tripathi, S. N., Eck, T., Newcomb, W., Slutsker, I., Dickerson, R., Thompson, A., Mattoo, S., Wang, S., Singh, R., Sinyuk, A., and Schafer, J.: Aerosol properties over the Indo–Gangetic plain: A1 mesoscale perspective from the TIGERZ experiment, J. Geophys. Res., 116, D18203, doi:10.1029/2011JD015809, 2011.
Giles, D. M., Holben, B. N., Eck, T. F., Sinyuk, A., Smirnov, A., Slutsker, I., Dickerson, R. R., Thompson, A. M., and Schafer, J. S.: An analysis of AERONET aerosol absorption properties and classifications representative of aerosol source regions, J. Geophys. Res., 117, D17203, doi:10.1029/2012JD018127, 2012.
Gopal Rama, K., Arafath, S. Md., Lingaswamy, A. P., Balakrishnaiah, G., Pavan Kumari, S., Uma Devi, K., Siva Kumar Reddy, N., Raja Obul Reddy, K., Penchal Reddy, M., Reddy, R. R., and Suresh Babu, S.: In-situ measurements of atmospheric aerosols by using Integrating Nephelometer over a semi-arid station, southern India, Atmos. Environ., 86, 228–240, 2014.

ACPD
14, 21101–21148, 2014

Guleria, R. P., Kuniyal, J. C., Rawat, P. S., Sharma, N. L., Thakur, H. K., Dhyani, P. P., and Singh, M.: The assessment of aerosol optical properties over Mohal in the northwestern Indian Himalayas using satellite and ground-based measurements and an influence of aerosol transport on aerosol radiative forcing, Meteorol. Atmos. Phys., 113, 153–169, doi:10.1007/s00703-011-0149-5, 2011.

Hegde, P. and Kawamura, K.: Seasonal variations of water-soluble organic carbon, dicarboxylic acids, ketocarboxylic acids, and α-dicarbonyls in Central Himalayan aerosols, Atmos. Chem. Phys., 12, 6645–6665, doi:10.5194/acp-12-6645-2012, 2012.

Hegde, P., Pant, P., Naja, M., Dumka, U. C., and Sagar, R.: South Asian dust episode in June 2006: aerosol observations in the central Himalayas, Geophys. Res. Lett., 34, L23802, doi:10.1029/2007GL030692, 2007.

Heintzenberg, J., Wiedensohler, A., Tuch, T. M., Covert, D. S., Sheridan, P., Ogren, J. A., Gras, J., Nessler, R., Kleefeld, C., Kalivitis, N., Aaltonen, V., Wilhelm, R. T., and Havlicek, M.: Intercomparison and aerosol calibrations of 12 commercial integrating Nephelometer of three manufacturers, J. Atmos. Ocean. Tech., 23, 902–914, 2006.

Hyvärinen, A.-P., Lihavainen, H., Komppula, M., Sharma, V. P., Kerminen, V.-M., Panwar, T. S., and Viisanen, Y.: Continuous measurements of optical properties of atmospheric aerosols in Mukteshwar, northern India, J. Geophys. Res., 114, D08207, doi:10.1029/2008JD011489, 2009.

Hyvärinen, A.-P., Raatikainen, T., Brus, D., Komppula, M., Panwar, T. S., Hooda, R. K., Sharma, V. P., and Lihavainen, H.: Effect of the summer monsoon on aerosols at two measurement stations in Northern India – Part 1: PM and BC concentrations, Atmos. Chem. Phys., 11, 8271–8282, doi:10.5194/acp-11-8271-2011, 2011a.

Hyvärinen, A.-P., Raatikainen, T., Komppula, M., Mielonen, T., Sundström, A.-M., Brus, D., Panwar, T. S., Hooda, R. K., Sharma, V. P., de Leeuw, G., and Lihavainen, H.: Effect of the summer monsoon on aerosols at two measurement stations in Northern India – Part 2: Physical and optical properties, Atmos. Chem. Phys., 11, 8283–8294, doi:10.5194/acp-11-8283-2011, 2011b.

Jayaraman, A., Gadhavi, H., Misra, A., Ganguly, D., Ramachandran, S., and Rajesh, T. A.: Spatial variations in aerosol characteristics and regional radiative forcing over India: measurements and modeling of 2004 road campaign experiment, Atmos. Environ., 40, 6504–6515, doi:10.1016/j.atmosenv.2006.01.034, 2006.

ACPD
14, 21101–21148, 2014

Kaskaoutis, D. G., Kalapureddy, M. C. R., Krishna Moorthy, K., Devara, P. C. S., Nastos, P. T., Kosmopoulos, P. G., and Kambezidis, H. D.: Heterogeneity in pre-monsoon aerosol types over the Arabian Sea deduced from ship-borne measurements of spectral AODs, Atmos. Chem. Phys., 10, 4893–4908, doi:10.5194/acp-10-4893-2010, 2010.

Kaskaoutis, D. G., Singh, R. P., Gautam, R., Sharma, M., Kosmopoulos, P. G., and Tripathi, S. N.: Variability and trends of aerosol properties over Kanpur, northern India using AERONET data (2001–10), Environ. Res. Lett., 7, 024003, doi:10.1088/1748-9326/7/2/024003, 2012.

Kaskaoutis, D. G., Sinha, P. R., Vinoj, V., Kosmopoulos, P. G., Tripathi, S. N., Misra, A., Sharmaf, M., and Singh, R. P.: Aerosol properties and radiative forcing over Kanpur during severe aerosol loading conditions, Atmos. Environ., 79, 7–19, doi:10.1016/j.atmosenv.2013.06.020, 2013.

Kaskaoutis, D. G., Kumar, S., Sharma, D., Singh, R. P., Kharol, S. K., Sharma, M., Singh, A. K., Singh, S., Singh, A., and Singh, D.: Effects of crop residue burning on aerosol properties, plume characteristics and longrange transport over northern India, J. Geophys. Res., 119, 5424–5444, doi:10.1002/2013JD021357, 2014.

Kirchstetter, T. W., Novakov, T., and Hobbs, P. V.: Evidence that the spectral dependence of light absorption by aerosols is affected by organic carbon, J. Geophys. Res., 109, D21208, doi:10.1029/2004JD004999, 2004.

Komppula, M., Lihavainen, H., Hyvärinen, A.-P., Kerminen, V.-M., Panwar, T. S., Sharma, V. P., and Viisanen, Y.: Physical properties of aerosol particles at a Himalayan background site in India, J. Geophys. Res., 114, D12202, doi:10.1029/2008JD011007, 2009.

Kopacz, M., Jacob, D. J., Fisher, J. A., Logan, J. A., Zhang, L., Megretskaia, I. A., Yantosca, R. M., Singh, K., Henze, D. K., Burrows, J. P., Buchwitz, M., Khlystova, I., McMillan, W. W., Gille, J. C., Edwards, D. P., Eldering, A., Thouret, V., and Nedelec, P.: Global estimates of CO sources with high resolution by adjoint inversion of multiple satellite datasets (MOPITT, AIRS, SCIAMACHY, TES), Atmos. Chem. Phys., 10, 855–876, doi:10.5194/acp-10-855-2010, 2010.

Kotamarthi, V. R. and Satheesh, S. K.: Ganges Valley Aerosol Experiment, Air & Waste Management Association, Em, The magazine for environmental managers, 2011.

Kumar, R., Barth, M. C., Pfister, G. G., Naja, M., and Brasseur, G. P.: WRF-Chem simulations of a typical pre-monsoon dust storm in northern India: influences on aerosol optical properties and radiation budget, Atmos. Chem. Phys., 14, 2431–2446, doi:10.5194/acp-14-2431-2014, 2014.

ACPD
14, 21101–21148, 2014

Lau, K. M., Kim, M. K., and Kim, K. M.: Asian summer monsoon anomalies induced by aerosol direct forcing: the role of the Tibetan Plateau, Clim. Dynam., 26, 855–864, doi:10.1007/s00382-014-2055-2, 2006.
Lawrence, M. G. and Lelieveld, J.: Atmospheric pollutant outflow from southern Asia: a review, Atmos. Chem. Phys., 10, 11017–11096, doi:10.5194/acp-10-11017-2010, 2010.
León, J.-F. and Legrand, M.: Mineral dust sources in the surroundings of the north Indian Ocean, Geophys. Res. Lett., 30, 1309, doi:10.1029/2002GL016690, 2003.
Liu, Z., Liu, D., Huang, J., Vaughan, M., Uno, I., Sugimoto, N., Kittaka, C., Trepte, C., Wang, Z., Hostetler, C., and Winker, D.: Airborne dust distributions over the Tibetan Plateau and surrounding areas derived from the first year of CALIPSO lidar observations, Atmos. Chem. Phys., 8, 5045–5060, doi:10.5194/acp-8-5045-2008, 2008.
Lu, Z., Zhang, Q., and Streets, D. G.: Sulfur dioxide and primary carbonaceous aerosol emissions in China and India, 1996–2010, Atmos. Chem. Phys., 11, 9839–9864, doi:10.5194/acp-11-9839-2011, 2011.
Manoharan, V. S., Kotamarthi, R., Feng, Y., and Cadeddu, M. P.: Increased absorption by coarse aerosol particles over the Gangetic–Himalayan region, Atmos. Chem. Phys., 14, 1159–1165, doi:10.5194/acp-14-1159-2014, 2014.
Manoj, M. G., Devara, P. C. S., Safai, P. D., and Goswami, B. N.: Absorbing aerosols facilitate transition of Indian monsoon breaks to active spells, Clim. Dynam., 37, 2181–2198, 2011.
Marcq, S., Laj, P., Roger, J. C., Villani, P., Sellegri, K., Bonasoni, P., Marinoni, A., Cristofanelli, P., Verza, G. P., and Bergin, M.: Aerosol optical properties and radiative forcing in the high Himalaya based on measurements at the Nepal Climate Observatory-Pyramid site (5079 m a.s.l.), Atmos. Chem. Phys., 10, 5859–5872, doi:10.5194/acp-10-5859-2010, 2010.
Nakajima, T., Yoon, S.-C., Ramanathan, V., Shi, G.-Y., Takemura, T., Higurashi, A., Takamura, T., Aoki, K., Sohn, B.-J., Kim, S.-W., Tsuruta, H., Sugimoto, N., Shimizu, A., Tanimoto, H., Sawa, Y., Lin, N.-H., Lee, C.-T., Goto, D., and Schutgens, N.: Overview of the atmospheric Brown Cloud East Asian Regional Experiment 2005 and a study of the aerosol direct radiative forcing in east Asia, J. Geophys. Res., 112, D24S91, doi:10.1029/2007JD009009, 2007.
Neitola, K., Asmi, E., Komppula, M., Hyvärinen, A.-P., Raatikainen, T., Panwar, T. S., Sharma, V. P., and Lihavainen, H.: New particle formation infrequently observed in Himalayan foothills – why?, Atmos. Chem. Phys., 11, 8447–8458, doi:10.5194/acp-11-8447-2011, 2011.

ACPD
14, 21101–21148, 2014

Pant, P., Hegde, P., Dumka, U. C., Sagar, R., Satheesh, S. K., Moorthy, K. K., Saha, A., and Srivastava, M. K.: Aerosol characteristics at a high-altitude location in central Himalayas: optical properties and radiative forcing, J. Geophys. Res., 111, D17206, doi:10.1029/2005JD006768, 2006.

Panwar, T. S., Hooda Rakesh, K., Lihavainen, H., Hyvärinen, A. P., Sharma, V. P., and Viisanen, Y.: Atmospheric aerosols at a regional background Himalayan site – Mukteshwar, India, Environ. Monit. Assess., 185, 4753–4764, doi:10.1007/s10661-012-2902-8, 2013.

Prabha, T. V., Karipot, A., Axisa, D., Padmakumari, B., Maheskumar, R. S., Konwar, M., Kulkarni, J. R., and Goswami, B. N.: Scale interactions near the foothills of Himalaya during CAIPEEX, J. Geophys. Res., 117, D10203, doi:10.1029/2011JD016754, 2012.

Raatikainen, T., Hyvärinen, A.-P., Hatakka, J., Panwar, T. S., Hooda, R. K., Sharma, V. P., and Lihavainen, H.: The effect of boundary layer dynamics on aerosol properties at the Indo–Gangetic plains and at the foothills of the Himalayas, Atmos. Environ., 89, 548–555, doi:10.1016/j.atmosenv.2014.02.058, 2014.

Ram, K. and Sarin, M. M.: Absorption coefficient and site-specific mass absorption efficiency of elemental carbon in aerosols over urban, rural, and high-altitude sites in India, Environ. Sci. Technol., 43, 8233–8239, 2009.

Ram, K. and Sarin, M. M: Spatio-temporal variability in atmospheric abundances of EC, OC and WSOC over Northern India, J. Aerosol Sci., 41, 88–98, doi:10.1016/j.jaerosci.2009.11.004, 2010.

Ram, K., Sarin, M. M., and Hedge, P.: Atmospheric abundances of primary and secondary carbonaceous species at two high-altitude sites in India: sources and temporal variability, Atmos. Environ., 42, 6785–6796, 2008.

Ram, K., Sarin, M. M., and Hegde, P.: Long-term record of aerosol optical properties and chemical composition from a high-altitude site (Manora Peak) in Central Himalaya, Atmos. Chem. Phys., 10, 11791–11803, doi:10.5194/acp-10-11791-2010, 2010.

Ramanathan, V., Chung, C., Kim, D., Bettge, T., Buja, L., Kiehl, J. T., Washington, W. M., Fu, Q., Sikka, D. R., and Wild, M.: Atmospheric brown clouds: impacts on South Asian climate and hydrological cycle, P. Natl. Acad. Sci. USA, 102, 5326–5333, doi:10.1073/pnas.0500656102, 2005.

Ramanathan, V., Li, F., Ramana, M. V., Praveen, P. S., Kim, D., Corrigan, C. E., Nguyen, H., Stone, E. A., Schauer, J. J., Carmichael, G. R., Adhikary, B., and Yoon, S. C.: Atmospheric

ACPD
14, 21101–21148, 2014

brown clouds: Hemispherical and regional variations in long-range transport, absorption, and radiative forcing, J. Geophys. Res., 112, D22S21, doi:10.1029/2006JD008124, 2007.
Randles, C. A. and Ramaswamy, V.: Absorbing aerosols over Asia: a geophysical fluid dynamics laboratory general circulation model sensitivity study of model response to aerosol optical depth and aerosol absorption, J. Geophys. Res., 113, D21203, doi:10.1029/2008JD010140, 2008.
Russell, P. B., Bergstrom, R. W., Shinozuka, Y., Clarke, A. D., DeCarlo, P. F., Jimenez, J. L., Livingston, J. M., Redemann, J., Dubovik, O., and Strawa, A.: Absorption Angstrom Exponent in AERONET and related data as an indicator of aerosol composition, Atmos. Chem. Phys., 10, 1155–1169, doi:10.5194/acp-10-1155-2010, 2010.
Sheridan, P. J. and Ogren, J. A.: Observations of the vertical and regional variability of aerosol optical properties over central and eastern North America, J. Geophys. Res., 104, 16793–16805, doi:10.1029/1999JD900241, 1999.
Sinha, P. R., Kaskaoutis, D. G., Manchanda, R. K., and Sreenivasan, S.: Characteristics of aerosols over Hyderabad in southern Peninsular India: synergy in the classification techniques, Ann. Geophys., 30, 1393–1410, doi:10.5194/angeo-30-1393-2012, 2012.
Srivastava, A. K., Tripathi, S. N., Dey, S., Kanawade, V. P., and Tiwari, S.: Inferring aerosol types over the Indo–Gangetic Basin from ground based sun photometer measurements, Atmos. Res., 109, 64–75, 2012.
Twardowski, M. S., Boss, E., Macdonald, J. B., Scott Pegau, W., Barnard, A H., and Zaneveld, J. R. V.: A model for estimating bulk refractive index from the optical backscattering ratio and the implications for understanding particle composition in case I and case II waters, J. Geophys. Res., 106, 14129–14142, 2001.
Vijayakumar, K. and Devara, P. C. S.: Influence of aerosol type, fine- and coarse-mode fractions on regional monsoon activity, Proc. INTROMET, 07–10 January 2014, Kattankulathur, 2014.
Vijayakumar, K., Devara, P. C. S., and Simha, C. P.: Aerosol features during drought and normal monsoon years: a study undertaken with multi-platform measurements over a tropical urban site, Aerosol Air Qual. Res., 12, 1444–1458, doi:10.4209/aaqr.2012.01.0005, 2012.
Virkkula, A., Backman, J., Aalto, P. P., Hulkkonen, M., Riuttanen, L., Nieminen, T., dal Maso, M., Sogacheva, L., de Leeuw, G., and Kulmala, M.: Seasonal cycle, size dependencies, and source analyses of aerosol optical properties at the SMEAR II measurement station in Hyytiälä, Finland, Atmos. Chem. Phys., 11, 4445–4468, doi:10.5194/acp-11-4445-2011, 2011.

ACPD
14, 21101–21148, 2014

Xu, C., Ma, Y. M., Panday, A., Cong, Z. Y., Yang, K., Zhu, Z. K., Wang, J. M., Amatya, P. M., and Zhao, L.: Similarities and differences of aerosol optical properties between southern and northern sides of the Himalayas, Atmos. Chem. Phys., 14, 3133–3149, doi:10.5194/acp-14-3133-2014, 2014.

ACPD
14, 21101–21148, 2014

Table 1. Details of AOS instruments, parameters and equations used for the calculation of aerosol optical properties. The bold-highlighted properties are examined in the current work.

Instruments	Primary measurements	Derived parameters	Equation
Three wavelength Nephelometer (TSI Model 3563)	Total scattering and hemispheric backscattering coefficients (σ_{sp} and σ_{bsp}) from D_1 and D_{10} particles at blue (0.45), green (0.55) and red (0.70) µm	**Hemispheric backscatter fraction**	$\boldsymbol{b = \sigma_{bsp}/\sigma_{sp}}$
		Scattering Ångström exponent	$\boldsymbol{\alpha_{sp} = -\log[\sigma_{sp}(\lambda_1)/\sigma_{sp}(\lambda_2)]/\log[\lambda_1/\lambda_2]}$
		Backscattering Ångström exponent	$\boldsymbol{\alpha_{sbs} = -\log[\sigma_{bsp}(\lambda_1)/\sigma_{bsp}(\lambda_2)]/\log[\lambda_1/\lambda_2]}$
		Up scatter fraction	$\beta = 0.0817 + 1.8495 \times b - 2.9682 \times b^2$
		Asymmetry parameter	$g = 1.011 - 1.036 \times \beta - 2.005 \times \beta^2$
		Single scattering albedo	$\omega = \sigma_{sp}/(\sigma_{sp} + \sigma_{ap})$
		Submicron scattering fraction	$\boldsymbol{R_{sp} = \sigma_{sp}(D_1)/\sigma_{sp}(D_{10})}$
		Hygroscopic growth factor	$f(\mathrm{RH}) = \sigma_{sp}(\mathrm{RH}_{85\%})/\sigma_{sp}(\mathrm{RH}_{40\%}) = ((1 - (\mathrm{RH}_{wet}/100))/(1 - (\mathrm{RH}_{dry}/100)))^{-\gamma}$
Radiance Research Particle Soot Absorption Photometer (PSAP)	Light absorption coefficient (σ_{ap}) from D_1 and D_{10} particles at blue (0.467), green (0.53) and red (0.66) µm	**Absorption Ångström exponent**	$\boldsymbol{\alpha_{ap} = -\log[\sigma_{ap}(\lambda_1)/\sigma_{ap}(\lambda_2)]/\log[\lambda_1/\lambda_2]}$
		Single scattering albedo	$\omega = \sigma_{sp}/(\sigma_{sp} + \sigma_{ap})$
		Submicron absorption fraction	$\boldsymbol{R_{ap} = \sigma_{ap}(D_1)/\sigma_{ap}(D_{10})}$

ACPD
14, 21101–21148, 2014

Table 2. Comparison of extensive and intensive aerosol properties over Nainital during GVAX campaign along with those measured over mountainous sites.

Sampling Site	Elevation (m)	Sampling Period	σ_{sp} (M m^{-1})	σ_{ap} (M m^{-1})	α_{sp}	α_{ap}	Reference
Nainital	1958	Jun 2011–Mar 2012	177.20 (104.40)*	10.90 (8.95)*	0.71 (1.21)*	1.07 (1.14)*	Present study
Nainital	1958	Feb 2005–Jul 2008	–	13.9	–	–	Ram et al. (2010)
Nainital	1958	Dec 2004	–	12.9	–	–	Ram and Sarin (2009)
Nainital	1958	Feb 2005–Jun 2007	–	12.2	–	–	Ram and Sarin (2009)
Mukteshwar	2180	Sep 2005–Sep 2007	53.00	11.00	–	1.0 to 1.6	Hyvärinen et al. (2009)
Mukteshwar	2180	Monsoon and Pre-Monsoon of year 2008	34.30–133.80	6.90–25.8	–	–	Hyvärinen et al. (2011b)
NCO-P	5079	Mar 2006 to Mar 2009	–	1.1	–	–	Marcq et al. (2010)
Mt. Abu	1700	Dec 2005–Feb 2006	–	8.0	–	–	Ram and Sarin (2009)
Mt. Abu	1700	May 2005–Feb 2006	–	5.8	–	–	Ram and Sarin (2009)

* Value inside parenthesis represents for $D_{1\,\mu m}$ size aerosols.

ACPD
14, 21101–21148, 2014

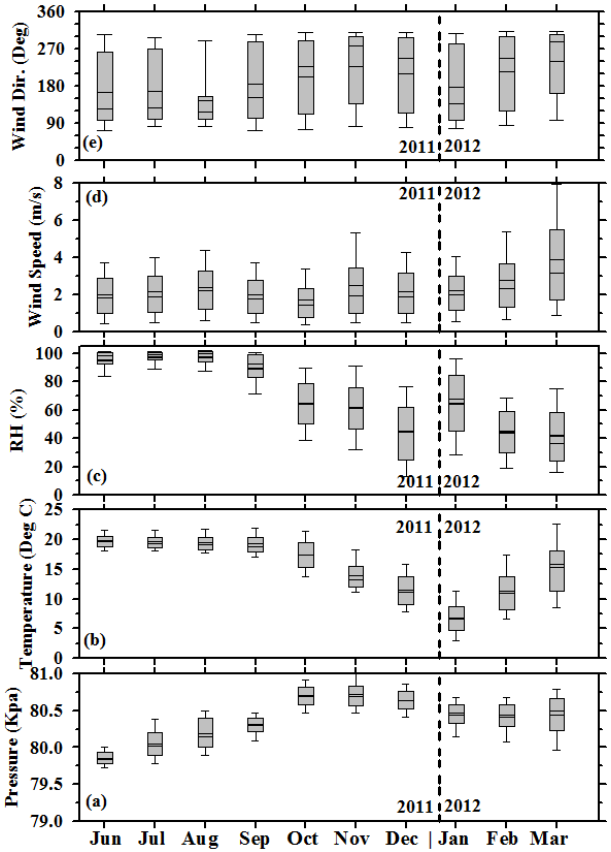

Figure 1. Monthly surface meteorological parameters (ambient pressure, air Temperature, Relative Humidity, wind speed and direction) at Nainital during the period June 2011 to March 2012 in box and whisker charts.

ACPD
14, 21101–21148, 2014

Scattering and absorption properties of near-surface aerosol

U. C. Dumka et al.

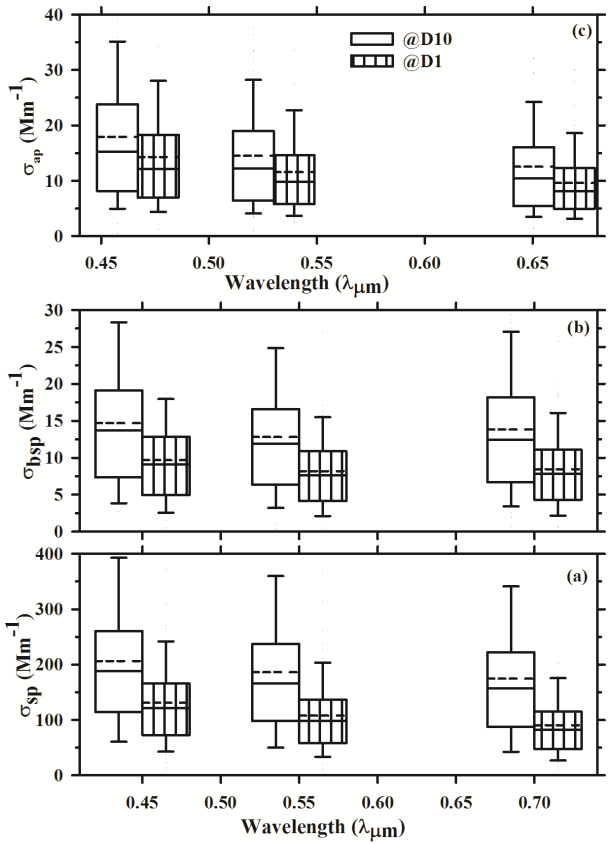

Figure 2. Statistical (box and whisker chart view) spectral distribution of **(a)** scattering coefficient (σ_{sp}), **(b)** back scattering coefficient (σ_{bsp}) and, **(c)** absorption coefficient (σ_{ap}) at Nainital during June 2011–March 2012. The dotted line represents the mean and the solid line the median. The box contains the range of values from 25 % (bottom) to 75 % (top).

ACPD
14, 21101–21148, 2014

Scattering and absorption properties of near-surface aerosol

U. C. Dumka et al.

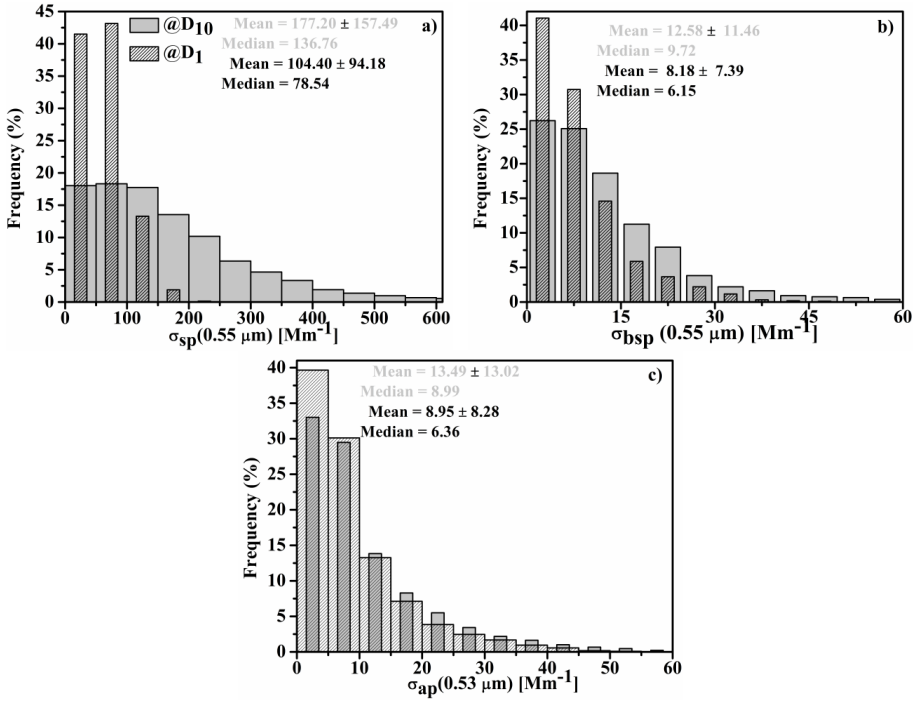

Figure 3. Frequency distribution of scattering coefficient **(a)** back scattering coefficient **(b)** and absorption coefficient **(c)** for $D_{1\,\mu m}$ and $D_{10\,\mu m}$ size groups.

ACPD
14, 21101–21148, 2014

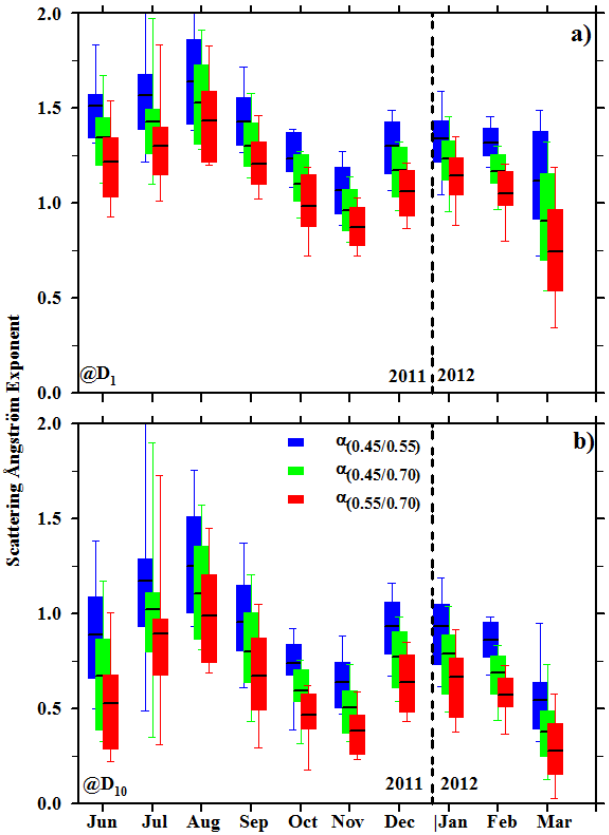

Figure 4. Monthly-mean variation of scattering Ångström exponent for $D_{1\,\mu m}$ **(a)** and $D_{10\,\mu m}$ **(b)** during June 2011 to March 2012. The box and whiskers denote the 95th and 5th percentiles, respectively. The box's upper and lower limits are 75th and 25th percentiles and black straight line shows the mean value. The vertical dotted line separates the years 2011 and 2012.

ACPD
14, 21101–21148, 2014

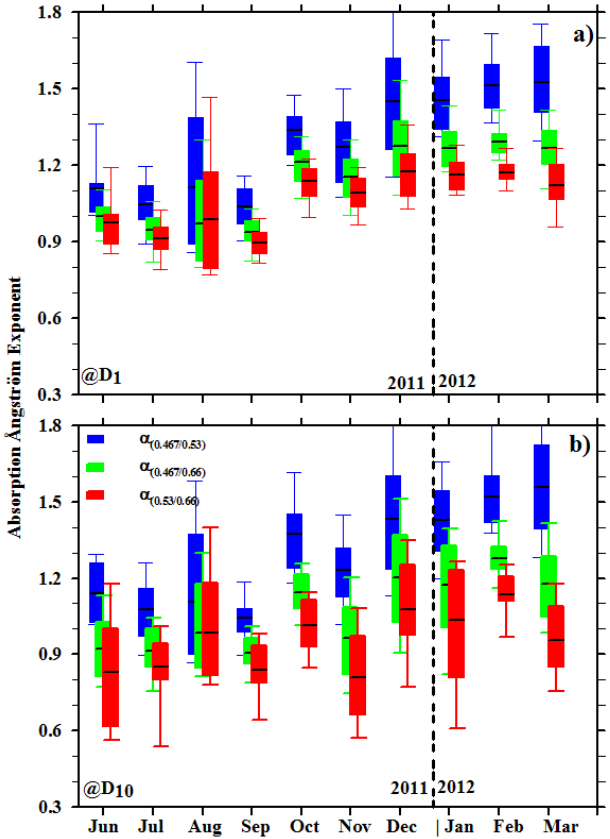

Figure 5. Same as in Fig. 4, but for the absorption Ångström exponent.

ACPD
14, 21101–21148, 2014

Scattering and absorption properties of near-surface aerosol

U. C. Dumka et al.

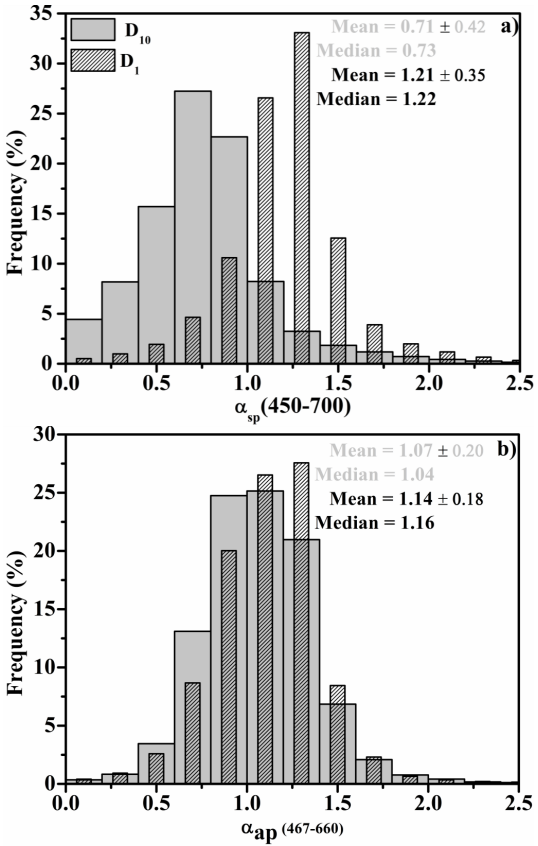

Figure 6. Frequency distribution of scattering Ångström exponent **(a)** and absorption Ångström exponent **(b)** for $D_{1\,\mu m}$ and $D_{10\,\mu m}$ size groups.

ACPD
14, 21101–21148, 2014

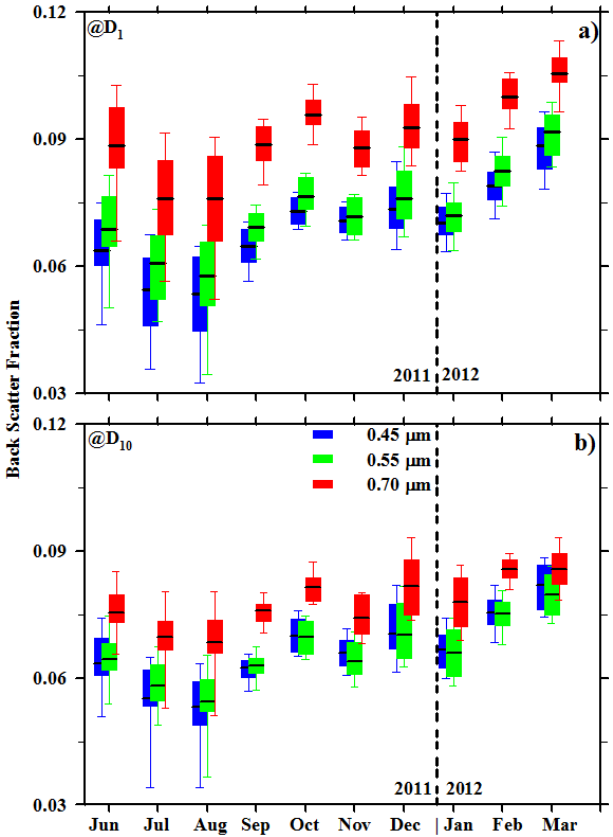

Figure 7. Same as in Fig. 4, but for the back-scatter fraction.

ACPD
14, 21101–21148, 2014

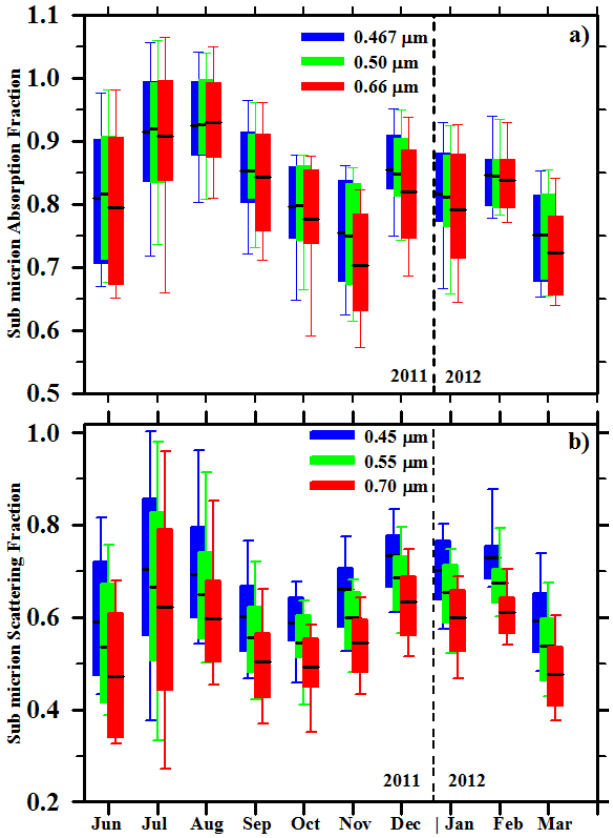

Figure 8. Same as in Fig. 4, but for the sub-micron absorption **(a)** and scattering **(b)** fraction.

ACPD
14, 21101–21148, 2014

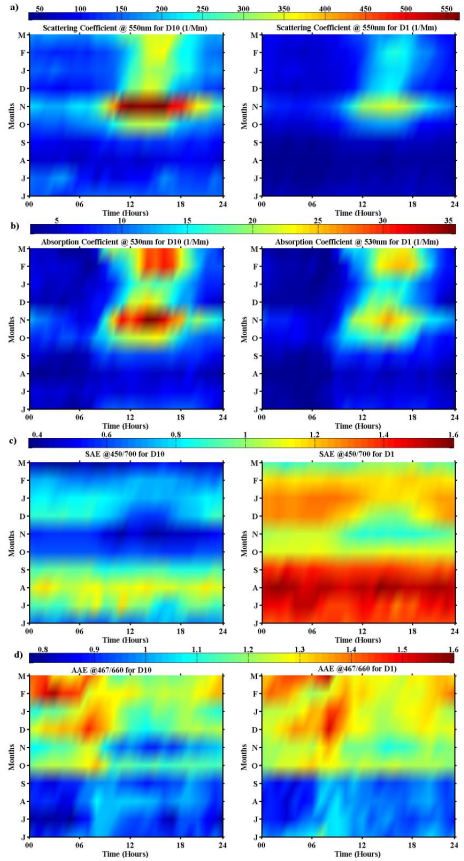

Figure 9. Monthly mean diurnal variation of **(a)** scattering coefficient, **(b)** absorption coefficient, **(c)** Scattering Ångström Exponent (SAE) and, **(d)** Absorption Ångström Exponent (AAE) for D_{10} and D_1 size particles.

ACPD
14, 21101–21148, 2014

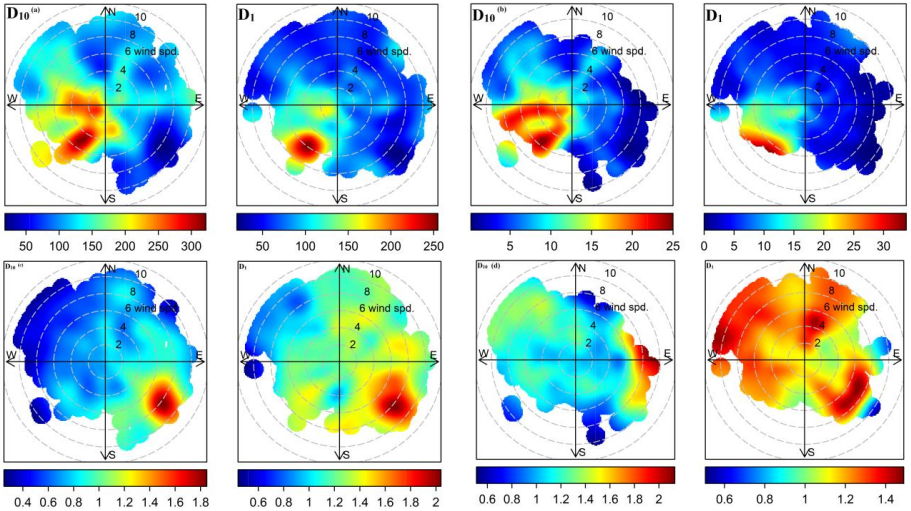

Figure 10. Bivariate plots of the scattering coefficient **(a)**, absorption coefficient **(b)**, scattering Ångström exponent **(c)** and absorption Ångström exponent **(d)** for $D_{10\,\mu m}$ and $D_{1\,\mu m}$ size groups.

ACPD
14, 21101–21148, 2014

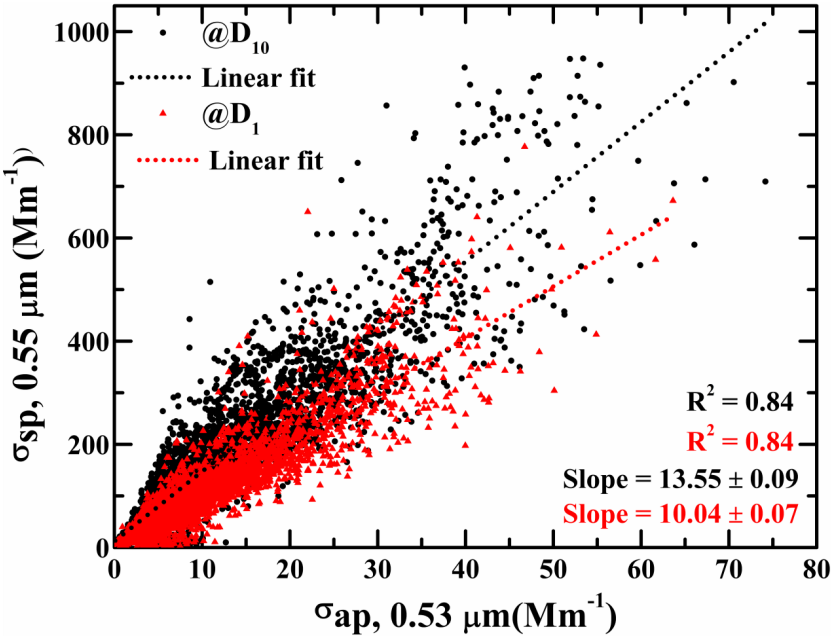

Figure 11. Correlation between the scattering and absorption coefficients for $D_{1\,\mu m}$ and $D_{10\,\mu m}$ particle-size groups.

ACPD
14, 21101–21148, 2014

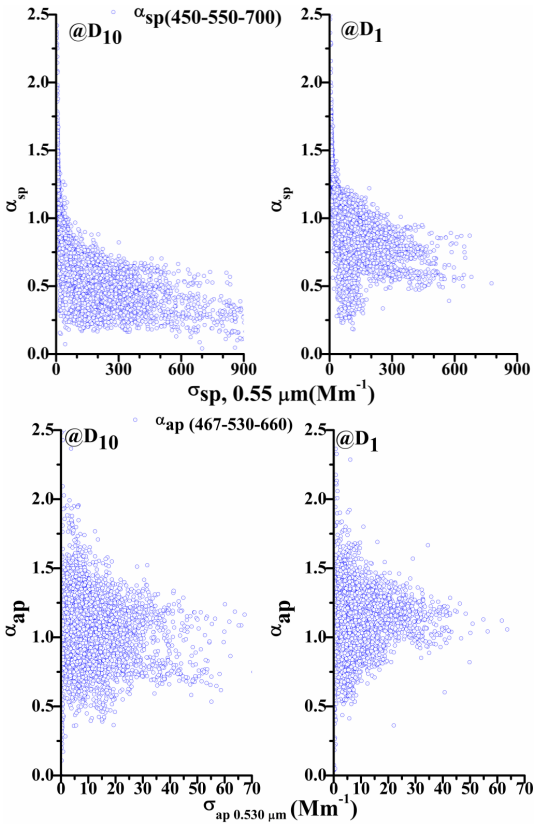

Figure 12. Correlation between the hourly-averaged values of the scattering coefficient with the scattering Ångström exponent (above) and for the absorption coefficient with the absorption Ångström exponent (below) for $D_{1\,\mu m}$ and $D_{10\,\mu m}$ particle-size groups.

ACPD
14, 21101–21148, 2014

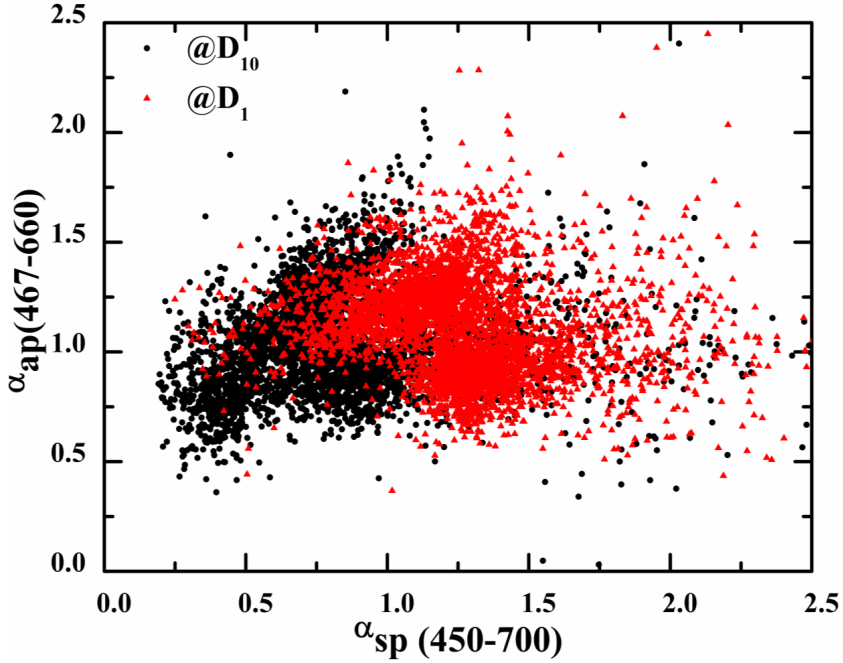

Figure 13. Correlation between scattering and absorption Ångström exponents (hourly-averaged values) at Nainital for $D_{1\,\mu m}$ and $D_{10\,\mu m}$ particle-size groups.

ACPD
14, 21101–21148, 2014